Am J Cancer Res 2021;11(7):3558-3574
www.ajcr.us /ISSN:2156-6976/ajcr0134923

Original Article

CR13626: a novel oral brain penetrant tyrosine kinase inhibitor that reduces tumor growth and prolongs survival in a mouse model of glioblastoma

Chiara Galimberti[1,2], Tiziana Piepoli[1], Ornella Letari[1], Roberto Artusi[1], Stefano Persiani[1], Gianfranco Caselli[1], Lucio C Rovati[1]

[1]Rottapharm Biotech Srl, Monza, Italy; [2]PhD Program in Neuroscience, University of Milano - Bicocca, Monza, Italy

Received May 5, 2021; Accepted June 4, 2021; Epub July 15, 2021; Published July 30, 2021

Abstract: Glioblastoma multiforme (GBM) is the most malignant primary brain cancer. Despite aggressive treatments currently there is no cure for GBM. Many challenges should be considered for the development of new therapeutical agents for glioblastoma, including appropriate target selectivity and pharmacokinetics. Several mutations and alterations of key cellular pathways including tyrosine kinases (TKs) are involved in malignant transformation and tumor progression. Thus, the targeting of multiple pathways and the development of innovative combination drug regimens is expected to yield improved therapies. Moreover, the abilities to cross the blood-brain barrier (BBB) reaching effective concentrations in brain and to remain into this tissue avoiding the effects of efflux transporters are also critical issues in the development of new therapeutics for GBM. CR13626 is a novel brain penetrant small molecule able to potently inhibit in vitro the activity of EGFR, VEGFR2 (aka KDR), Fyn, Yes, Lck, HGK (aka MAP4K4) and RET kinases relevant for GBM development. CR13626 shows good oral bioavailability (72%) and relevant brain penetration (brain/plasma ratio of 1.4). In an orthotopic xenograft glioblastoma mouse model, oral treatment with CR13626 results in a time-dependent reduction of tumor growth, leading to a significant increase of animal survival. The unique properties of CR13626 warrant its further investigation as a potential new drug candidate in glioblastoma.

Keywords: Glioblastoma, multikinase inhibitors, blood-brain barrier, orthotopic implantation, CR13626, tumor spheroids

Introduction

The relevance of glioblastoma (GBM) in the global panorama of cancer research is highlighted by the high number of reviews on it: 127 reviews in the first two months of 2021 are indexed in PubMed.

Among them, the review of Oronsky et al. summarizing the characteristics of newly diagnosed GBM, the current standard of care, and potential new therapeutics is relevant to the aim of the present paper [1].

Indeed, GBM is the most malignant type of primary brain cancer. It represents half of all new diagnoses of glioma and is classified by the World Health Organization as a grade IV astrocytoma [2]. Prognosis and survival rates remain poor, with a median patient survival of less than 15 months from diagnosis [3-5] and a five-year survival of 5.6% [6]. Moreover, GBM is by far the worse tumor in terms of average of lost life years, i.e., 20.1 lost years vs., for instance, 15.1 and 12 lost years for melanoma and pancreatic carcinoma, respectively [7].

According to the current treatment guidelines, first-line treatment consists of multistep treatments including surgery plus radiotherapy with concurrent and adjuvant temozolomide (TMZ) (Stupp regimen) [1, 3]. Unfortunately, these approaches are never conclusive, the recurrence is almost universal, and the management of recurrent GBM remains challenging due to the limited availability of treatment options [1].

The high grade of cellular proliferation, invasiveness, cellular atypia, and angiogenesis contribute to the poor prognosis of GBM. These fea-

tures depend largely upon the activity of cell surface membrane receptors, the receptor tyrosine kinases (RTKs) [8, 9]. Upon activation of the receptors, members of Src-family kinases (SFKs) are recruited and involved in the intracellular signal transmission, contributing to GBM tumorigenesis and tumor cell motility, invasion, and angiogenesis [10].

The epidermal growth factor receptor (EGFR) is the most frequent amplified gene in malignant glioma, present in approximately 40% of GBM cases [11]. The heterogeneity of EGFR alterations in GBM, including the constitutively activated truncated variant III (EGFRvIII), are object of a vast literature, identifying EGFR as a promising target for GBM treatment [12]. However, clinical trials based on the specific inhibition of EGFR in GBM gave disappointing results [12-15]. Several reasons are associated with these failures, including the concomitant expression of EGFR mutant and wild-type forms, the development of resistance in recurrent tumors upon therapy, the compensatory activation of other RTKs, and the adverse effects arising from the collateral inhibition on wild-type EGFR in normal tissues.

The aberrant activation of EGFR signaling pathways affects cellular proliferation, migration, and differentiation and induces the inhibition of apoptosis and the upregulation of vascular endothelial growth factor (VEGF) expression, leading to angiogenesis [16]. VEGF is strongly induced by hypoxia and acts through three receptor tyrosine kinases (VEGFRs), among which the major player is the vascular endothelial receptor 2 (VEGFR2, aka KDR), which is also involved in sustaining GBM cell viability and proliferation [17]. The treatment with anti-angiogenic agents seems to give some advantages in counteracting GBM tumor. Firstly, it has been demonstrated in several clinical trials that compounds inducing a normalization of abnormal tumor vessels, rather than a "vessel blockade", may translate in clinical benefits, although with significant differences between individual patients [18-20]. Secondly, anti-angiogenic therapeutics may disrupt the link between tumor-vasculature and tumor stem-like cells located in perivascular niches and surrounded by endothelial cells [18]. Finally, VEGF/VEGFR targeted therapies may have an immune-supportive effect if combined with immune checkpoint inhibitors, by switching an immunologically "cold" tumor into a "hot" one [21].

Even though potent inhibitors of EGFR and VEGFR2 pathways have been shown to be highly effective in several solid tumors, their role in controlling GBM has been disappointing. One explanation of these failures is the poor ability to cross the BBB [22]. Indeed, even if GBM tumor leads to a partial disruption of the BBB by constituting the leakier blood-brain tumor barrier (BBTB), this phenomenon is mainly observed at the core of the tumor, not close to the infiltrative areas responsible of tumor recurrence [23, 24]. Thus, highly permeable compounds, reaching both the tumor core and the distant sites of invasion, are needed for an effective GBM treatment.

As mentioned above, the development of resistance to a single agent therapy and the intrinsic heterogeneity of the tumor contribute to the failure of new therapeutics for GBM. The use of kinase inhibitors able to simultaneously block different key players in tumor development, the so-called multikinase approach, could allow the overcoming of these obstacles, as described by Frantz [25]. Indeed, several multikinase inhibitors hit the market (e.g., sorafenib, sunitinib, pazopanib, anlotinib, levantinib, regorafenib) and demonstrated therapeutic efficacy in some cancers.

Herein we present the early pharmacological characterization of CR13626, a novel multikinase inhibitor endowed with a unique pattern of inhibition on kinases relevant for GBM. Indeed, CR13626 inhibits EGFR and VEGFR2 tyrosine receptor kinases, the members of Src-family kinases (SKFs) Fyn, Yes and Lck, and some emerging kinases involved in GBM, such as HGK (MAP4K4) and RET. CR13626 is also characterized by surprisingly favorable pharmacokinetic properties (i.e., high oral bioavailability and the ability to cross the BBB). These favorable characteristics support further development of CR13626 as a new drug candidate in glioblastoma.

Materials and methods

In vitro kinase selectivity screen

CR13626 inhibitory activity against a panel of 173 kinases was assessed at Eurofins Cerep laboratories (Celle-Lévescault, France) in accor-

dance with Eurofins validation Standard Operating Procedures. Enzyme assays were performed in duplicate under optimized conditions for each enzyme. The potency of CR13626 was assessed by determining the IC_{50} values of the percent inhibition dose response curves obtained by testing CR13626 in the concentration range of 0.001-1 μM.

Cell lines and culture conditions

The human glioblastoma cells lines were obtained as follow: U87MG and T98G cell lines were from ATCC, the U373 cell line was from ECACC and the U87 MG vIII cell line was purchased from Celther Polska. Cells were cultured in DMEM medium supplemented with 10% FBS and 1% Pen-Strep (U87, T98G and U373) or in MEM medium supplemented with 10% FBS, 1% Pen-Strep, 0.2% Gentamycin and 200 μg/ml G418 (U87 MG vIII) at 37°C with 5% CO_2.

The human embryonic kidney 293 cells (HEK-293, from ATCC) were cultured in DMEM medium supplemented with 10% FBS at 37°C with 5% CO_2. The human Umbilical Vein Endothelial Cells (HUVEC-C, from ATCC) were grown in medium F12K + 0.1 mg/ml Heparin + 0.05 mg/ml ECGS + 10% FBS at 37°C with 5% CO_2.

Cellular phosphorylation assays

VEGF-induced VEGFR2 (Y1175)-phosphorylation: HUVEC-C cells were plated at 6×10^4 cells/well in 24 w microplates. After 24 hours, starvation was induced overnight in medium F12K + 0.1 mg/ml Heparin + 0.5% FBS (medium starvation). At the end, cells were treated for 1 hour with CR13626 or reference compound (axitinib, SellekChem, #S1005) diluted in medium starvation (DMSO 0.1% final concentration) and then stimulated for 5 min with VEGF stimuli (Sigma, #V7259, 50 ng/ml final concentration in medium starvation). At the end, cell lysates were obtained as described above. 15 μl of each sample were separated by SDS-PAGE followed by transfer to a PVDF membrane. Membranes were blocked as reported and probed overnight with primary antibodies specific to phospho-VEGFR2 (p-Tyr1175, Cell Signaling, #2478), VEGFR2 (Cell Signaling, #9698), phospho-Fyn/Src (p-Tyr416, Cell Signaling, #2101), Fyn (Cell Signaling, #4023) or Actin (ThermoFisher, #MA5-11869). Membranes were washed and protein bands visualized using appropriate HRP-conjugated secondary antibodies and chemiluminescent detection. Densitometric analysis of sample lanes were performed by ImageQuant TL software (GE Healthcare Life Sciences). Each sample value was normalized by respective actin and the relative level of protein phosphorylation was determined by normalizing the phosphoprotein signal to that of the total protein.

EGF-induced EGFR (Y1068)-phosphorylation: U87MG cells were seeded at 3×10^5 cells/well in 12 w microplates. After 24 hours, starvation was induced overnight in medium DMEM + 0.1% FBS (medium starvation). At the end, cells were treated for 1 hour with CR13626 or reference compound (erlotinib, Sigma, #CDS022564) diluted in medium starvation (DMSO 0.1% final concentration) and then stimulated for 15 min with EGF (Sigma, #E9644, 10 ng/ml final concentration in medium starvation). At the end, cells were lysed in M-PER lysis buffer containing 1× Protease/Phosphatase inhibitors cocktail (Cell Signaling, #5872S) and samples were sonicated. 10 μg of total protein were separated by SDS-PAGE followed by transfer to a PVDF membrane. Membranes were blocked with Blocking buffer (Thermo Scientific #37542) and probed overnight with primary antibodies specific to phospho-EGFR (p-Tyr1068, Cell Signaling, #2234), EGFR (Cell Signaling, #2239) or Actin (ThermoFisher, #MA5-11869). Membranes were washed and protein bands visualized using appropriate HRP-conjugated secondary antibodies and chemiluminescent detection. Densitometric analysis of sample lanes were performed by ImageQuant TL software and the relative level of protein phosphorylation was determined as described above.

Tau phosphorylation upon Fyn activation: HEK-293 cells were seeded at 6×10^5 cells/well in 12 w microplates coated with poly-D-lysine hydrobromide (PDL). The day after, the expression of both FynB and Tau proteins was induced for 24 hours through the co-transfection of cells with the respective encoding vectors by using the Lipofectamine 3000 Transfection Reagent (Life Technologies, # L3000_008). At the end of the incubation, medium was replaced and the treatment with CR13626 or the reference saracatinib (both

diluted in medium DMEM + 10% FBS, DMSO 0.1% final concentration) was performed for 24 hours. At the end, lysates of cells were then obtained by adding M-PER lysis buffer, sonicated, and stored at -80°C. Phosphorylation of Tau was investigated by a customized indirect-ELISA as follow. Lysates were diluted in coating buffer (Sigma, #C3041) at the concentration of 30 µg/ml; 3 µg/100 µl/well of total protein were coated overnight in a 96w plate (NUNC Maxisorp). At the end, wells were washed 3× in PBST, then blocked in PBS-1% BSA for 1 hour at room temperature with gentle shaking. Wells are then washed 3× in PBST and incubated with the primary antibodies specific to phospho-Tau (p-Tyr18, MediMabs, #MM-0194-P) or anti-total Tau (Sigma Aldrich, #MAB2239) for 2 hours at room temperature with gentle shaking. After 3× washing with PBST, wells were incubated for 1 hour with the HRP-conjugated anti-mouse secondary antibodies (Jackson Immuno Research, #115-035-071) and gentle shacked. At the end, wells were washed 3× in PBST and 100 µl/well of HRP-substrate TMB (3,3',5,5'-tetramethylbenzidine) were added. The colorimetric reaction was stopped by adding sulfuric acid, and the signal was measured at 450 nm by Multiskan FC Microplate Photometer (ThermoFisher Scientific). The effect of the compounds was calculated by using the ratio P-Tau/Tot-Tau of treated wells compared to controls (not treated cells) and expressed as percentage. The IC_{50} values were calculated by GraphPad Prism Software.

In vitro endothelial cell tube-formation assay

The assay was performed using HUVEC-C cells and the tube formation assay kit (Abcam, #ab204726). Briefly, 50 µl/well of the extracellular matrix solution (ECM) were added to an empty 96 w culture plate and incubated for 1 hour at 37°C to allow the solution to form a gel. Then, 2×10^4 cells/100 µl were seeded to each well, followed by the addition of 25 µl/well of a 100× mix solution containing PMA stimuli (phorbol 12-myristate 13-acetate, Sigma, #P1585) +/- inhibitors (CR13626, axitinib, erlotinib and vinblastine) in medium F12K + Heparin 0.1 mg/ml + FBS 5% (DMSO 0.1% final concentration). Cells were incubated for 18 hours at 37°C with 5% CO_2 to allow tube formation. At the end, cells were washed once and stained according to the manufacturer's instructions. The formation of vessels-like structures was examined using light microscopy by EVOS microscope.

Cell proliferation assays

2D cultures: The effects of CR13626 on cellular proliferation were investigated in different human GBM cell lines (U87MG, U373, U87MG vIII) as 2D cultures by ViaCount assay (Millipore). 2×10^4 cells/well were plated in a 24 w in DMEM 10%. After 72 hours the cells are treated with the CR13626 for 24, 72 h or 7 days, with a medium replacement on day 4. At the end of the incubation the analysis was performed according to kit instructions.

3D spheroids: The effects of CR13626 on cellular proliferation were assessed in U87MG 3D spheroids. First, U87MG tumor cells spheroids were grown in MW96 CELLCARRIER SPHEROID ULA-96 plates. 1500 cells/well were seeded in medium containing or not CR13626 and incubated for 72 hours. At the end spheroids were analyzed by the CellTiter Glo 3D Cell Viability assay (Promega), according to kit instructions.

Pharmacokinetic studies

In vitro study (Caco-2 cell assay): Caco-2 cells plates were purchased from Areta international S.r.l. (Gerenzano, Italy). Cells were seeded on the polycarbonate microporous filters (0.4 µm of pore diameter) of 24 HTS Transwell plates (Becton and Dickinson, now ThermoFisher Scientific) and grown for 21 days to reach confluence. To evaluate the monolayers integrity, a Trans epithelial electrical resistance (TEER) was measured in each well. At the end of the experiment, monolayers integrity was checked through the calculation of the Lucifer yellow (LY) marker paracellular permeability by fluorescence detection (excitation and emission wavelengths of 410 and 535 nm, respectively). LY paracellular flux lower than 0.7% after 1 hour of incubation and/or a permeability lower than 1×10^{-6} cm/s were considered acceptable. CR13626 working solution was prepared at 10 µM in HBSS (containing Ca^{2+}, Mg^{2+} and 10 mM Hepes, pH 7.4). Atenolol (poorly permeable), labetalol (moderately permeable) and propranolol (highly permeable) were also prepared at 10 µM in HBSS (final DMSO < 1%) and tested as reference compounds.

Compounds were applied either to the apical (A) or the basolateral (B) side of the cell monolayer (upper or lower compartment of the insert, respectively) and the apical-to-basolateral (A→B) and basolateral-to-apical (B→A) transports were evaluated by quantifying compounds at the basal and apical sides over 1.5 hours of incubation at 37°C by HPLC-MS/MS. The A→B and B→A apparent permeability (Papp), B→A/A→B ratio and A→B and B→A mass balances were calculated.

In vivo studies: All animal studies described in this paper comply with the ARRIVE guidelines. Absolute bioavailability of CR13626 was investigated in male CD1 mice (Charles River, 29-33 g weight, 5 weeks old), after single oral administration. CR13626 was dissolved in 5% DMSO in phosphate buffer pH 7 (150 mM), 0.1% Tween 80 and 5% Cremophor EL and intravenously or orally administered at 3 mg/kg. Blood and brain samples were collected before dosing and at 0.08 (IV only), 0.25, 0.5, 1, 2, 4, 6, and 24 hours post dosing (3 animals per time point). Approximately 500 µL of blood were taken from retro-orbital plexus under deep anesthesia (2% isoflurane in pure oxygen) and collected in tubes with anticoagulant. Samples were centrifuged and plasma was stored at -80°C. CR13626 was extracted from plasma through a protein precipitation method by adding 200 µL of methanol to 20 µL of plasma in 96-deep well plates (Greiner), followed by mixing and centrifugation for 15 min at 3700 rpm at 4°C. To determine CR13626 concentrations in brain, each mice brain was removed, washed twice in saline solution, dried with blotting paper, weighted, cut in half, and frozen at -80°C. One hemisphere was weighted and homogenized through acoustic disruption (Covaris AFA S2), by adding a volume of acidic solution (formic acid 0.1% in water) corresponding to three times the weight (ml/g) of the hemisphere. Each homogenized-containing tube was processed with 6 repeated cycles of the following two run conditions: 1) 20 sec. 50% duty cycle, 1 0 intensity, 1000 cycles/burst, and 2) 1 0 sec. 50% duty cycle, 10 intensity, 100 cycles/burst. Then, 30 µL of the extracted solution were added to 0.23 mL of methanol, mixed and centrifuged for 5 min at 13500 rpm at 4°C. The supernatant was transferred to a 96-deep well plate (Axygen).

The determination of CR13626 in plasma and brain samples was assessed by liquid chromatography-tandem mass spectrometry (LC-MS/MS) on an API 4000 Qtrap ESI instrument in the positive ion mode.

PK parameters were calculated by the Phoenix 64 WinNonlin software using non-compartmental methods.

The dose proportionality of CR13626 pharmacokinetics in male CD1 mice (Charles River, 27-31 g weight, 5 weeks old) was evaluated after single oral administration in the dose range from 3 to 100 mg/kg. In this experiment, CR13626 was suspended in 0.5% HPMC solution (HPMC E4M Premium, Colorcon), 3 animals per time point were evaluated. Blood and brain samples were obtained as above described and collected before dosing and at 0.25, 0.5, 1, 2, 4, 6, 24 hours post dose. Determination of CR13626 concentration by LC-MS/MS was performed as above described.

Orthotopic mouse model of GBM

The study was performed at Accelera Srl laboratories (Nerviano, Italy). The protocol A14D6.EXT.16 was approved by the Italian Authorities. Human GBM U87MG cells (source ATCC) were engineered to express the luciferase gene, Luc2 (pGL4, Promega). On the implantation day (Day 0), U87MG-luc cells (1×10^6/2 µl of PBS), were injected into the brain (right hemisphere) of athymic nude (Hsd:AthymicNude-Foxn1nu) male mice from Charles River aged 5 weeks (23.6-32.2 g weight). Briefly, anesthetized mice (zoletil + xilor 2% anesthesia) were placed under the stereotaxic apparatus, gently fixed with ear bars into the head holder, and then the right coordinates for injection were chosen (+ 0.5 mm anterior and + 2.2 mm lateral, right). A small burr hole was done by a microdrill and cells were injected at 3 mm depth. The burr hole was closed using bone wax and the wound closed with sterile autoclips. Mice, after surgery were monitored until wakening and complete recovery from anesthesia. Eight days from tumor cell implantation, mice were subjected to the first bioluminescence (BLI) detection. According to the BLI values, animals were randomized and distributed into four experimental groups (8 mice/group). The oral treatment with CR13626 started on day 9 post implantation and continued for 10 days at the dose of 50 mg/kg/daily. Tumor growth was evaluated by in vivo BLI measurements at the

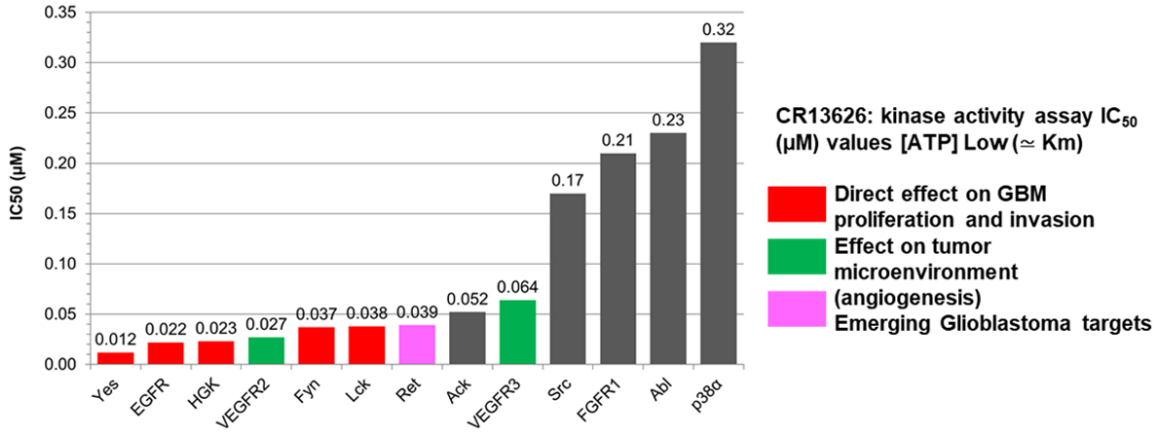

Figure 1. Potency of CR13626 against a set of tyrosine kinases relevant for GBM.

end of dosing (day 19) and during follow-up (days 26 and 33).

Survival of animals was also evaluated. Mice were monitored daily for mortality and clinical signs (including body weight). Toxicity was evaluated based on body weight reduction and signs of distress caused by the treatment. Animal survival was assessed using a Kaplan-Meier survival curve and Mantel-Cox test was used to determine differences between groups. The analysis was performed using GraphPad Prism (GraphPad Software Inc.).

Satellite group: six mice intracranially injected with the U87MG-luc cells were treated orally for 5 days with CR13626 (50 mg/kg/daily) or vehicle, starting from Day 37 post cell injection and sacrificed 3 hours after the last dosing. Plasma and brain samples were collected and analyzed to determine CR13626 concentrations by LC-MS/MS as already described.

Ethical approval

All procedures performed in studies involving animals were in accordance with the current Italian legislation (legislative Decree March 4th, 2014 n. 26) enforcing the EU Directive 2010/63/EU on the protection of animals for biomedical research. All the studies were approved by Italian authorities.

Results

Target identification

CR13626 was tested in a screening panel of 173 kinases and showed a sub nanomolar inhibitory activity on different kinases involved in the progression of glioblastoma, including members of RTK and Src family kinases (see **Figure 1**).

In addition, CR13626 displayed a slight inhibitory effect (>70% at 1 μM) on other kinases, such as PDGFRα (platelet-derived growth factor receptor α) and CDK6 (cyclin-dependent kinase 6) (Tables S1, S2, S3).

Interestingly, when CR13626 was tested at higher concentrations of ATP (0.5 mM, i.e., intracellular ATP concentrations), the VEGFR2 IC_{50} value did not significantly change, maintaining the nanomolar inhibition of the kinase, thus confirming CR13626 inhibitory activity also in physiological cell conditions (data not shown).

CR13626 biochemical characterization on selected kinases

Upon activation of tyrosine kinase receptors, several residues located in the intracellular domain of the receptors were phosphorylated, leading to the recruitment of downstream effectors that mediate signal into the cell and activate specific biological pathways. Given the above-mentioned inhibitory activity of CR13626 towards some RTKs (i.e., EGFR and VEGFR2) and Fyn kinase, the ability of CR13626 to inhibit those enzymes was evaluated in different cellular models (**Figure 2**).

The effect of CR13626 on VEGFR2 activation was determined in HUVEC-C cells using axitinib

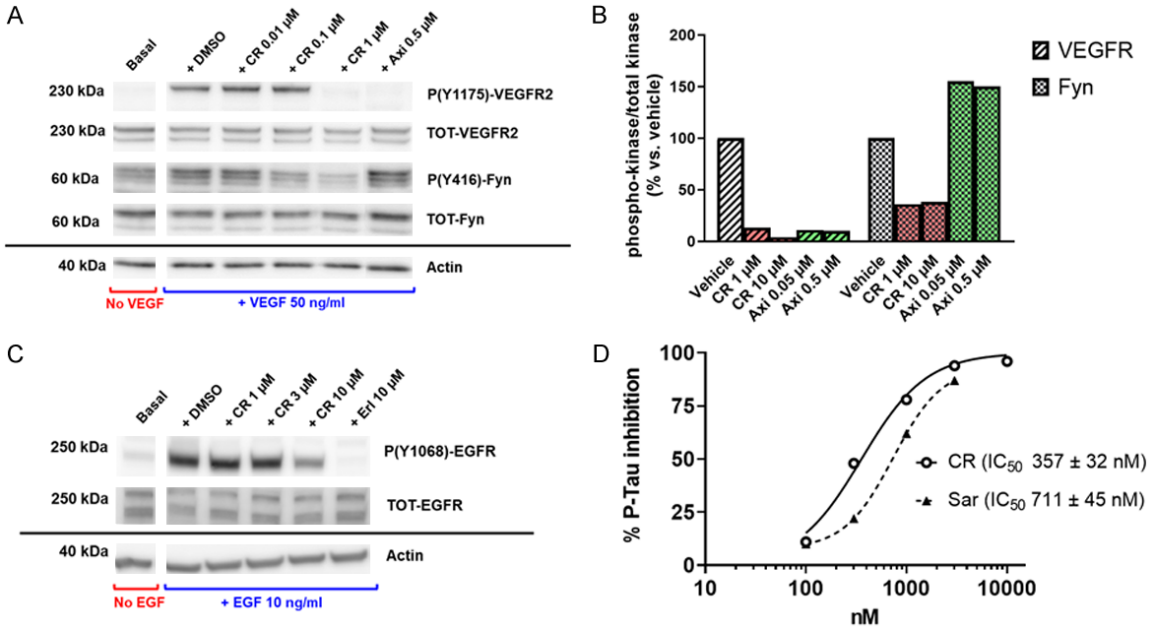

Figure 2. CR13626 reduces the ligand-induced phosphorylation of VEGFR2, EGFR and Fyn-mediated phosphorylation of Tau in a concentration dependent manner. A. Immunoblot analysis of VEGFR2 phosphorylation on tyrosine residue 1175 (P(Y1175)), total VEGFR2 (TOT-VEGFR2), Fyn/Src phosphorylation on tyrosine residue 416 (P(Y416)), total Fyn (TOT-Fyn) and Actin (loading control) in human HUVEC-C cell lysates. Cells were serum-starved overnight and then treated with DMSO 0.1% or indicated compounds (CR13626, CR and axitinib, Axi) for 1 hour. Cells were then stimulated with 50 ng/ml VEGF for 5 min. (full gel images in Figure S1). B. Densitometric analysis of VEGFR2 and Fyn/Src immunoblot images. C. Immunoblot analysis of EGFR phosphorylation on tyrosine residue 1068 (P(Y1068)), total EGFR (TOT-EGFR), and Actin (loading control) in human GBM U87MG cell lysates. Cells were serum-starved overnight and then treated with DMSO 0.1% or indicated compounds (CR13626, CR and erlotinib, Erl) for 1 hour. Cells were then stimulated with 10 ng/ml EGF for 15 min. (full gel images in Figure S2). D. A representative graph describing the activity of CR13626 (CR) compared to saracatinib (Sar) on Tau phosphorylation at Y18 residue (IC_{50} values ± SEM, duplicate data points) in Fyn/Tau over-expressing HEK-293 cells. The treatment of cells with CR13626 or saracatinib was performed for 24 hours.

as standard VEGFR inhibitor. CR13626 inhibits the ligand-induced receptor activation at residue Y1175 in a concentration dependent manner, reaching a total signal inhibition at 1 µM (**Figure 2A**). As expected, axitinib also inhibits the VEGFR2 phosphorylation induced by VEGF, but it does not show any effects on the downstream activation of Fyn/Src, probably due to the presence of collateral pathways. On the contrary, CR13626 also inhibits the Fyn/Src phosphorylation, suggesting a potential stronger impact on the intracellular signal transmission upon VEGFR activation (**Figure 2A**, **2B**).

The effect of CR13626 on EGFR activation was determined in the human GBM cell line U87MG using erlotinib as standard EGFR inhibitor. CR13626 inhibits the ligand-induced receptor activation at residue Y1068 in a concentration dependent fashion, with an IC_{50} value of 3 µM (**Figure 2C**).

To better define the potency of CR13626 on Fyn kinase in a cellular model, we exploit the assessment of the Fyn-mediated phosphorylation levels of Tau in Fyn/Tau co-transfected HEK-293 cells. Indeed, it has been demonstrated that Fyn kinase is specifically responsible of the phosphorylation of Tau at the tyrosine residue 18 (Y18) and this modification is present in the neurofibrillary tangles in Alzheimer's disease (AD) brain, giving to Fyn a fundamental role during the neurodegenerative process of AD [26]. Saracatinib was also tested and used as reference inhibitor of Fyn. As represented in **Figure 2D**, after 24 hours of treatment, CR13626 inhibits the phosphorylation of Tau at Y18 residue, with an IC_{50} value of 357 nM, 2-fold more active than the reference saracatinib. This effect has been confirmed in several experiments: the IC_{50} values (mean ± SD) were 417 ± 46 nM for CR13626 (n=4) and 800 ± 331 nM for saracatinib (n=3).

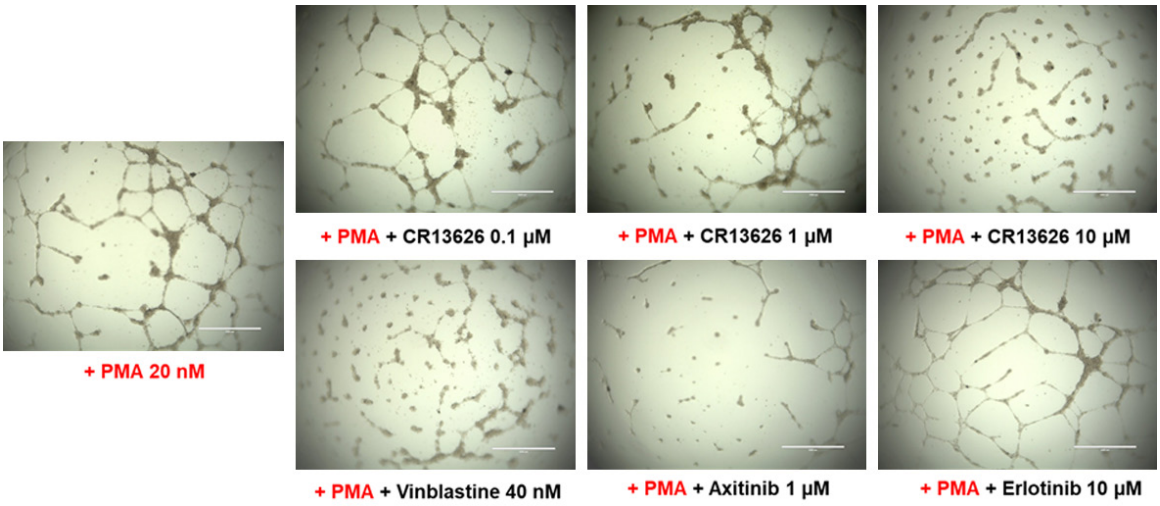

Figure 3. CR13626 reduces the PMA-induced tube-like structures formation in a concentration dependent manner. Representative phase-contrast images of HUVEC-C tube formation on ECM after 18 hours of treatment. Scale bar =1000 µm.

CR13626 effect on angiogenesis

We evaluated the ability of CR13626 to reduce the formation of new vessel-like structures in a HUVEC-C tube formation assay, as an indication of its antiangiogenic properties (**Figure 3**). It has been demonstrated that PMA-induced tube formation is reduced by inhibiting the VEGF receptor kinase, or by VEGF knockdown [27]. Vinblastine (inhibitor of microtubule formation [28]), and axitinib (VEGFR inhibitor [29]) were used as reference inhibitors, whereas erlotinib (EGFR inhibitor) was included as negative control. CR13626 decreases the PMA-induced tube formation in a dose-dependent manner, indicating a potential effect of the compound on the angiogenic process.

CR13626 effect on cellular proliferation

CR13626 preferentially reduces the proliferation of the U87MG human GBM cells with respect to non-tumor cells (**Figure 4A**). The treatment with CR13626 1 µM leads to more than 50% decrease of the viability of U87MG cells at 24 hours of incubation. Conversely, when CR13626 has been tested in the same conditions on a non-tumor human cell line HEK-293, it did not show any effect on cellular proliferation, as illustrated in **Figure 4A**. The ability of CR13626 to reduce the proliferation of U87MG cell line was then compared to that of erlotinib (EGFR inhibitor) [30] and saracatinib (Src family inhibitor) [31] after 6-7 days of treatment. CR13626 shows a higher efficacy than erlotinib, while the Src family inhibitor saracatinib resulted inactive (**Figure 4B**).

Besides the effect described above on U87MG cells, we tested the effect of CR13626 on the proliferation of three other human GBM cell lines (U373, U87MG vIII and T98G) cultured as 2D. These cell lines harbor some of the genetic alterations/mutations present in GBM tumor cells.

U373 cells share with U87MG cells the expression of the wild-type form of EGFR but, if the latter has deletions in PTEN and CDKN2A/2B genes, the former holds the amplification of PDGFRα and VEGFR2. Thus, the U87MG and U373 cells differ significantly in their gene expression fingerprints and show phenotypes resembling the neuronal and mesenchymal characters of GBM, respectively [32].

U87MG vIII cells express high levels of the constitutive active mutant form of EGFR, called EGFRvIII. This activated form results from the deletion of exon 2-7 in the extracellular domain of the EGFR receptor and is the most frequent deletion occurring in GBM. Wild type EGFR and EGFRvIII elicit differential signaling cascades; it has been demonstrated that EGFR amplification is acquired early by GBM cells, contributing to invasive processes. Then, upon tumor progression, GBM cells acquire EGFRvIII mutations which contribute to the angiogenic switch and a more aggressive tumor growth [12]. Finally, T98G are TMZ resistant cell line [33].

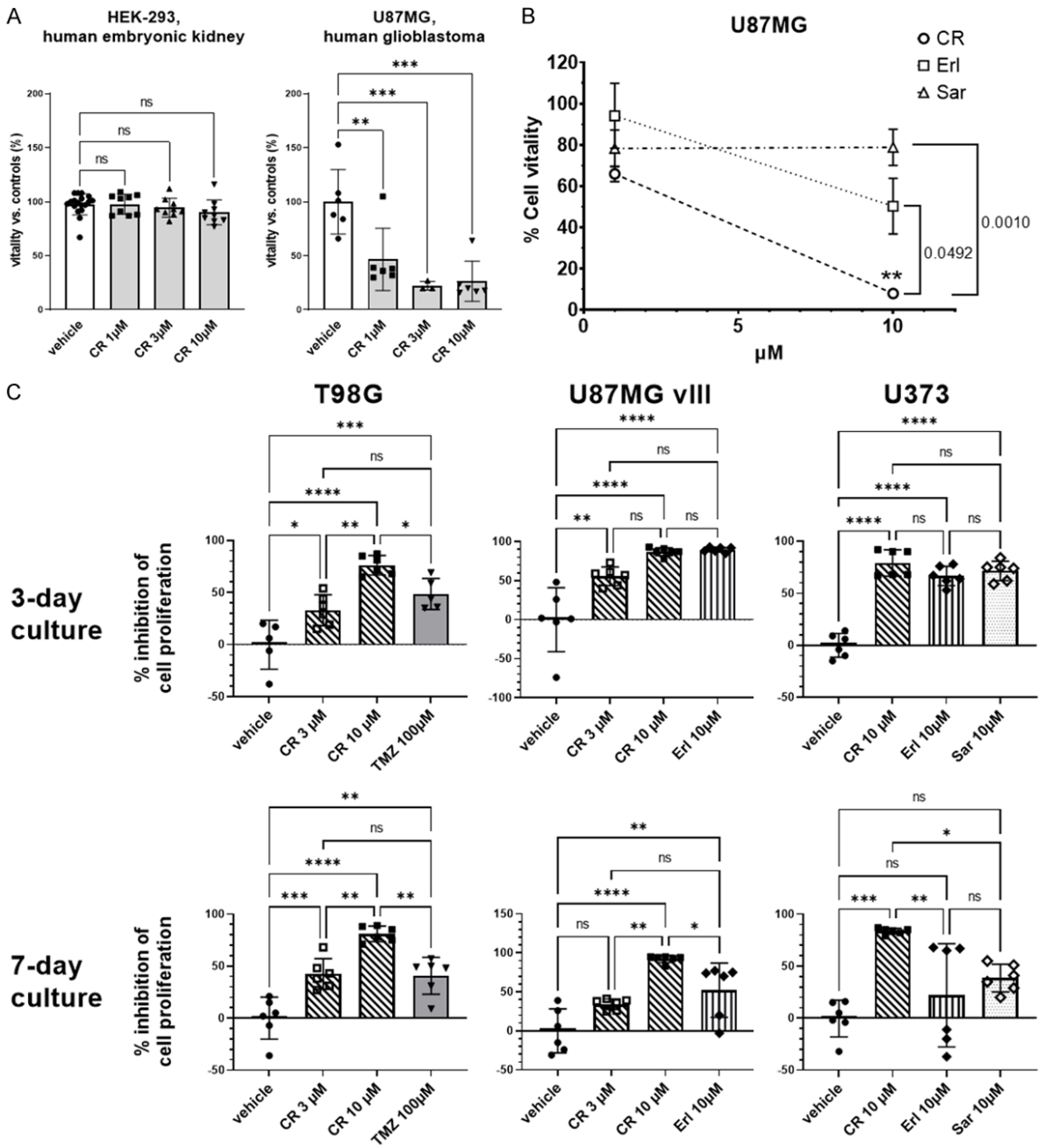

Figure 4. Effect on cellular proliferation. A. Effect of CR13626 (CR) on U87MG human GBM cells compared to HEK-293 cells. Percent of residual cell vitality in the presence of CR13626 (single values and mean ± SD), 24 hours of treatment). **P < 0.01; ***P < 0.001 by one-way ANOVA. B. Effect on U87MG human GBM cells of CR13626 compared with erlotinib (Erl) and saracatinib (Sar). Cells were treated for 6-7 days (medium replacement at day 4). Data are expressed as mean ± SEM, n=6, **P < 0.01 vs. vehicle (100% ± 10.5); on the right *p* values at 10 μM vs. comparators "Brown-Forsythe and Welch's ANOVA test". C. Effect of CR13626 on different human GBM cell lines: T98G (TMZ resistant), U87MG vIII (constitutively activated EGFR form), and U373 (mesenchymal GBM features). CR13626 was tested in comparison with temozolomide (TMZ), erlotinib (Erl) and saracatinib (Sar). Percent of inhibition of proliferation after 3 or 7 days of treatment. Single values and mean ± SD. **P < 0.01; ***P < 0.001 by one-way ANOVA and Tukey test.

CR13626 reduces the proliferation of all the cells cited above, being more effective than comparators. Moreover, the effect of CR13626 resulted still present after 7 days of treatment (**Figure 4C**).

3D cell spheroids are more representative of the complexity of tumor environment with respect to 2D cultures representing a more reliable model to assess cellular response to a drug treatment. Therefore, the efficacy of

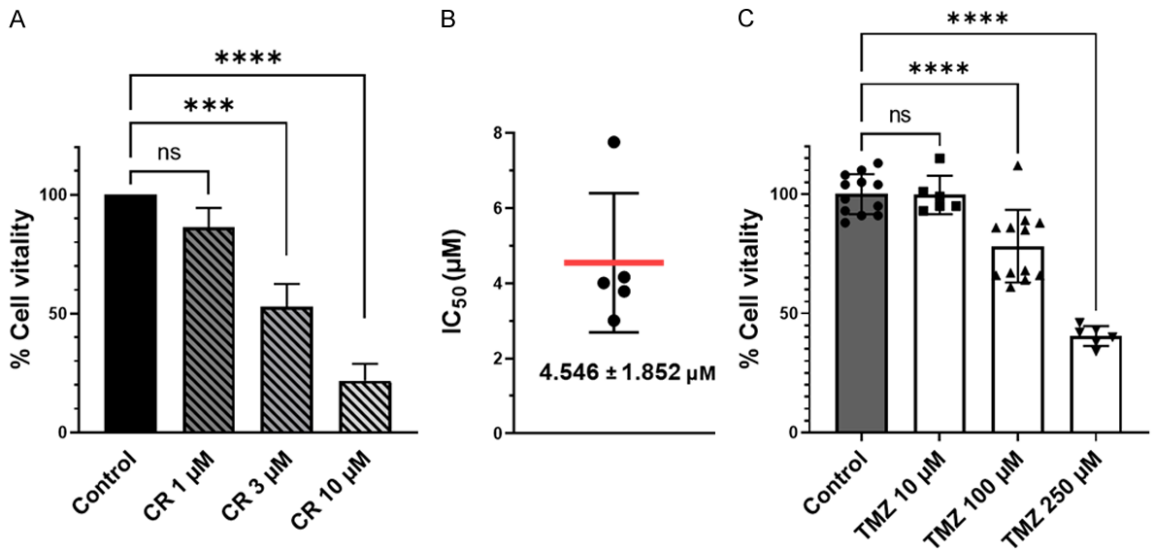

Figure 5. CR13626 (CR) reduces the proliferation of U87MG GBM cell lines grown as 3D spheroids. A. Percent of residual cell vitality of U87MG cells in presence of CR13626 (mean ± SEM of 5 experiments performed with n=5-6 spheroids/condition, 3 days of treatment). ***P < 0.001; ****P < 0.0001 by one-way ANOVA. B. IC_{50} values, single values and mean ± SD. C. Effect of temozolomide (TMZ). The graph reports the single spheroid values (percent of residual cell vitality in the presence of TMZ, 3 days of treatment) from two combined experiments and the mean ± SD; ****P < 0.0001 by one-way ANOVA.

Table 1. CR13626 in vitro transport rate evaluation

Papp (A→B) (cm/s × 10^{-6})	Papp (B→A) (cm/s × 10^{-6})	(B→A)/(A→B) ratio	Efflux	Mass balance A→B (%)	Mass balance B→A (%)
17.5	5.3	0.3	NO	85	76

CR13626 in reducing cellular proliferation was also evaluated in U87MG cells cultured as 3D spheroids after 3 days of treatment. CR13626 decreases the proliferation of U87MG cells in a dose-dependent fashion, showing an IC_{50} value of 4.5 µM (**Figure 5A**, **5B**). In the same culture conditions, the standard of care TMZ is also able to reduce U87MG spheroids proliferation, even if at higher concentrations with respect to CR13626. This is reflected by the calculated IC_{50} value of temozolomide (approximately 1.5 mM), **Figure 5C**.

CR13626 pharmacokinetic properties in CD1 and tumor bearing mice

To estimate the CR13626 in vivo permeability across the intestinal tract, the in vitro transport rate of CR13626 across the Caco-2 cells monolayer membrane was evaluated. CR13626 was tested at the concentration of 10 µM and the transports in the apical to basolateral (A→B) and in the basolateral to apical (B→A) directions were determined according to the method described above. The obtained results are summarized in **Table 1**. CR13626 could be classified as a medium permeability drug both in the apical-to-basolateral (A→B) and basolateral-to-apical (B→A) directions. Moreover, CR13626 is not a substrate of P-gp and BCRP multidrug efflux transporters, which are involved in brain tumor drug resistance.

The pharmacokinetics and brain exposure of CR13626 were assessed in plasma and brain homogenate tissues of CD1 mice and tumor-bearing nude mice.

The pharmacokinetics of CR13626 after single intravenous (IV) and oral (PO) administration at the dose of 3 mg/kg was evaluated in CD1 mice (**Figure 6A**, **6B**). CR13626 shows good oral absolute bioavailability (72%) and relevant brain penetration (brain/plasma ratio of 1.4), as reported in **Table 2**.

The dose proportionality of CR13626 pharmacokinetics after single oral administration in

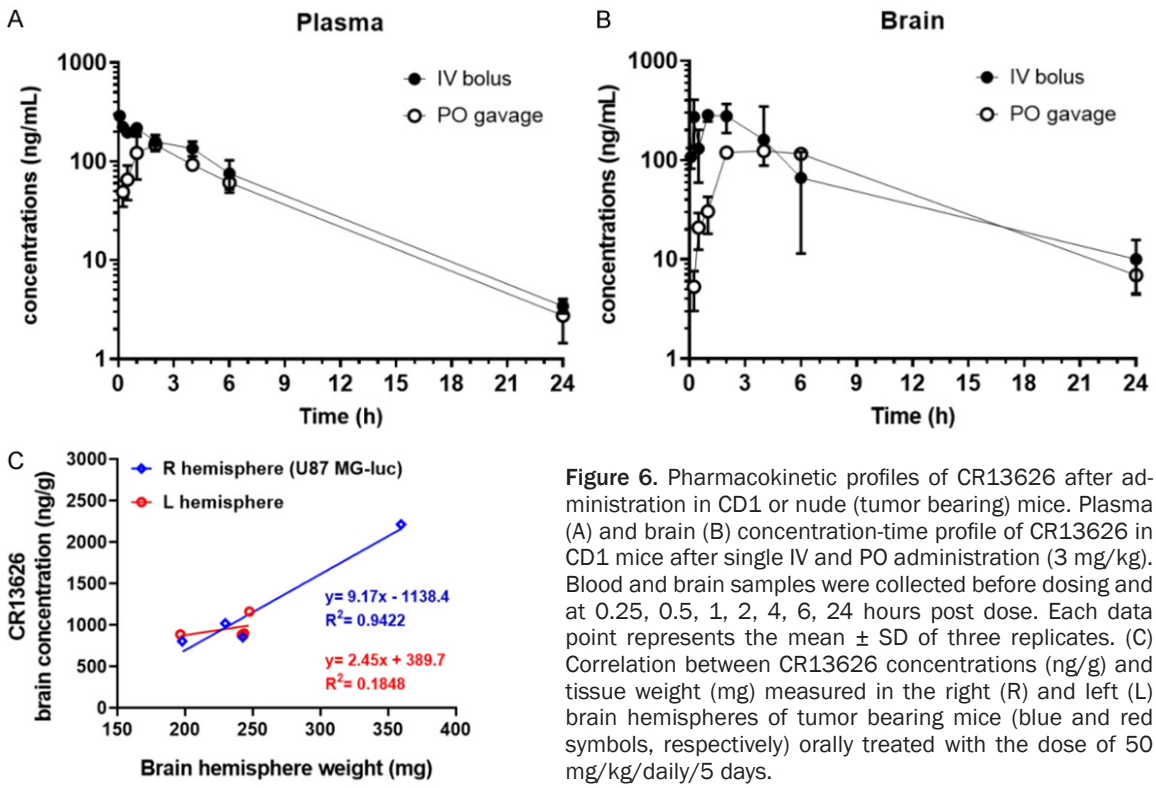

Figure 6. Pharmacokinetic profiles of CR13626 after administration in CD1 or nude (tumor bearing) mice. Plasma (A) and brain (B) concentration-time profile of CR13626 in CD1 mice after single IV and PO administration (3 mg/kg). Blood and brain samples were collected before dosing and at 0.25, 0.5, 1, 2, 4, 6, 24 hours post dose. Each data point represents the mean ± SD of three replicates. (C) Correlation between CR13626 concentrations (ng/g) and tissue weight (mg) measured in the right (R) and left (L) brain hemispheres of tumor bearing mice (blue and red symbols, respectively) orally treated with the dose of 50 mg/kg/daily/5 days.

Table 2. CR13626 pharmacokinetic parameters in plasma and brain of CD1 mice treated with 3 mg/kg by the intravenous (IV) or the oral (PO) way

CR13626 (3 mg/kg)	Plasma					Brain					B/P ratio
	T_{max} (hours)	C_{max} (ng/ml)	AUC (ng*h/ml)	$t_{1/2}$ (hours)	F	T_{max} (hours)	C_{max} (ng/g)	AUC (ng*h/g)	$t_{1/2}$ (hours)	F	
IV	0.08	-	1643	3.87	-	1	-	1951	NA	-	1.2
PO	2	147	1183	3.98	72%	2	119	1676	4.8	86%	1.4

Parameters were estimated by curve fitting of all individual data (n=3 observations per time point). AUC: Area under the curve; B/P: Brain/Plasma.

the dose range from 3 to 100 mg/kg in CD1 mice was also evaluated. Within the dose-range tested, CR13626 shows linear exposure as evidenced in **Table 3** (C_{max}/dose and AUC/dose columns), demonstrating that its pharmacokinetics are independent of the administered dose.

The brain tropism of CR13626 was also evaluated in tumor bearing mice treated orally once a day for five consecutive days at the dose of 50 mg/kg. CR13626 plasma and brain tissues concentrations were obtained at 3 hours from the last dose (i.e., the time necessary for CR13626 to reach the maximum brain concentration in CD1 mice, **Figure 6B**). The results confirm the brain tropism of CR13626, and the exposure observed in CD1 mice (please compare **Tables 4** and **2**). Moreover, CR13626 preferentially accumulates in the right hemisphere, where the U87MG-Luc cells were injected, and tumor developed (**Figure 6C**). This confirms the ability of CR13626 to cross the BBB and penetrate the brain, suggesting the potential of CR13626 to reach the tumor and remain at the tumor site.

CR13626 antitumor efficacy in an orthotopic mouse model of GBM

The in vivo antitumor activity of CR13626 was determined in a mouse model of GBM obtained by the orthotopic injection of U87 MG-Luciferase (U87 MG-Luc) GBM cells in nude mice. CR13626 oral treatment started on day 9 post-implantation and continued for 10 days

Table 3. Dose-proportionality of CR13626 pharmacokinetics in plasma and brain of CD1 mice treated with ascending oral doses

CR13626 (mg/kg)	Plasma (P)						Brain (B)						B/P ratio
	T_{max} (h)	C_{max} (ng/ml)	AUC (ng*h/ml)	$t_{1/2}$ (h)	C_{max}/ dose	AUC/ dose	T_{max} (h)	C_{max} (ng/g)	AUC (ng*h/g)	$t_{1/2}$ (h)	C_{max}/ dose	AUC/ dose	
3	2	147	1183	3.98	49	394	2	119	1676	4.8	40	559	1.4
10	2	597	4352	5.71	60	435	2	895	10523	5.3	90	1052	2.4
30	1	1520	14693	3.82	51	490	2	1233	14509	4.9	41	484	1.0
100	1	3860	37060	5.95	39	371	4	4182	66832	8.3	42	668	1.8

Parameters were estimated by curve fitting of all individual data (n=3 observations per time point). AUC: Area under the curve; B/P: Brain/Plasma.

Table 4. CR13626 concentrations (ng/g) in tumor bearing nude mice

Nude Mouse ID (50 mg/kg)	Plasma (ng/ml) (at 3 h)	Brain right hemisphere (tumor bearing)		Brain left hemisphere (tumor free)	
		(ng/g)	Brain/Plasma ratio	(ng/g)	Brain/Plasma ratio
4707	698	1020	1.46	1163	1.67
4715	352	2213	6.29	888	2.52
4719	399	852	2.14	881	2.21
4731	536	804	1.5	901	1.68
Mean	496.25	1222.25	2.85	958.25	2.02
SD	155.51	666.96	2.32	136.75	0.42

Compound's concentrations (ng/g) and tissue weight (mg) values were measured in right (R) and left (L) brain hemispheres of tumor bearing nude mice (n=4). CR13626 oral treatment was 50 mg/kg/daily/5 days. 3 h after the last dose all mice were euthanized, plasma and brain tissues collected, and the two brain hemispheres separated. Samples were analyzed by LC-MS/MS.

(50 mg/kg/daily). This treatment schedule was chosen as a stringent protocol to allow the assessment of the activity of CR13626, if present, avoiding false positive results.

Bioluminescence (BLI) measurements show a time-dependent reduction of tumor growth in the CR13626-treated group, reaching 60% on the last BLI evaluation 33 days post-implantation (i.e. 15 days after the end of dosing), as illustrated in **Figure 7A**. Due to the high variance, no statistics could be attempted on radiance data.

After the last BLI measurements, animals were monitored to assess survival. Tumor growth inhibition translated into an increase of 25% of the median survival time of animals treated with CR13626 compared to the vehicle group ($P<0.05$), **Figure 7B**. The observed antitumor effects agreed with the exposure of tumor-bearing mice to CR13626, which was above the TKs in-vitro IC_{50} values.

Discussion

To date, there is no cure for glioblastoma, the most malignant type of primary brain cancer. The first-line treatment options are limited, and recurrence of the tumor is almost universal. Thus, the unmet medical needs for GBM are extremely high and many efforts are ongoing to find a more effective therapy that provides survival benefit.

The pathogenesis of gliomas involves sequential accumulation of genetic alterations and abnormal regulation of growth factor signaling pathways that result in malignant transformation [11]. Tumor heterogeneity and the presence of the blood brain barrier (BBB), with efflux transporters, are some of the causes of failure of novel therapeutic agents. Thus, appropriate target selectivity and pharmacokinetics (including brain penetration) are critical issues for the generation of potential drug candidates.

In this paper we describe the pharmacology of CR13626 as a new small molecule inhibiting a set of kinases which play a fundamental role in GBM development.

Glioma's growth, progression, and proliferation, as well as the angiogenesis process, depend largely upon the activity of receptor tyrosine kinases [2]. CR13626 inhibits EGFR receptor, one of the main players involved in the GBM tumor pathophysiology, by affecting cell proliferation, migration, differentiation, and inducing angiogenesis through VEGF expression [11].

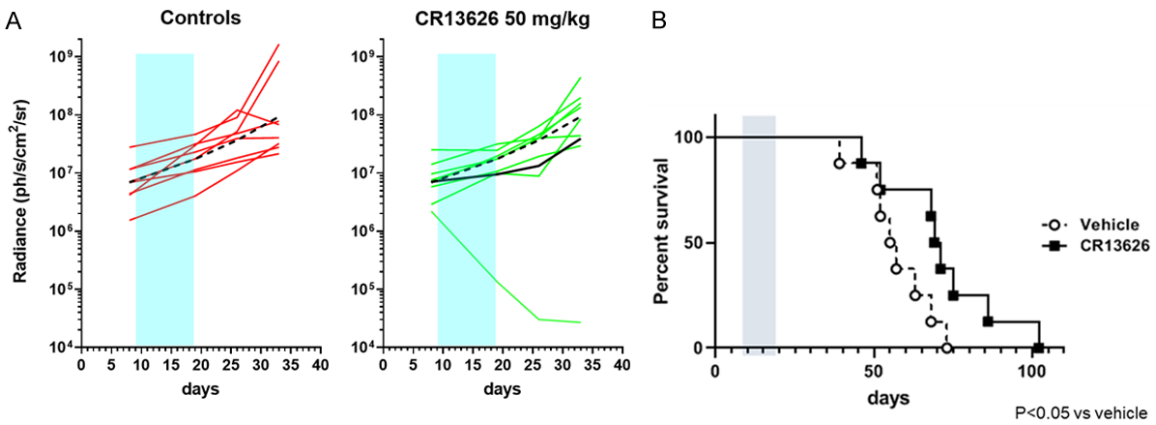

Figure 7. CR13626 treatment leads to a time-dependent reduction of tumor growth and to a significant increase of the survival of animals in a U87MG-Luc mouse model of GBM. A. CR13626 effect on tumor growth. Randomization of animals was performed (n=8/group) according to bioluminescence (BLI) values at day 8 after U87 MG-Luc injection (mean values at randomization of 9×10^6 ph/s/cm^2/sr). One day later, animal started oral administration of vehicle or CR13626 (50 mg/kg/daily/10 days, shaded area). Tumor progression was evaluated through the measurement of BLI at the end of dosing (day 19) and during follow-up (days 26-33). BLI is expressed as Radiance (ph/s/cm^2/sr). Individual values and geometric mean (black line, continuous CR13626, dotted Controls). B. Survival curves of CR13626 (50 mg/kg/daily/10 days) vs. vehicle. Animal survival was evaluated using a Kaplan-Meier survival curve. *P < 0.05 by Mantel-Cox test. Dosing of CR13626 started on day 9 and lasted 10 days only (shaded area).

Despite the failure of many drugs against EGFR alterations, due to the resilience of EGFR amplification and the presence of EGFRvIII form in GBM, the targeting of EGFR axis is still considered as valid [15]. CR13626 reduces the proliferation of the U87MG and U87MG vIII cell lines, which harbor the amplification of EGFR and the expression of the constitutive active mutant form EGFRvIII, respectively. Importantly, CR13626 is also able to inhibit the proliferation of U87MG cells cultured as 3D spheroids.

GBM invasion into the surrounding structures is associated with the angiogenesis process, which is induced by the release of VEGF, as a consequence of hypoxia. More recently it has been demonstrated that a specific VEGFR2 variant (Q472H) is a predictor of MGMT promoter methylation and, therefore, of TMZ resistance [34]. CR13626 inhibits VEGFR2 receptor and reduces the formation of new vessel-like structures in a concentration-dependent way.

Upon activation of RTKs, the signal is transmitted up to the nucleus through several intracellular kinases. Src-family kinases (SFKs) play a central role in many key GBM features [35]. Increased SFKs activity mediates tumorigenesis and is critical for GBM cell motility, invasion, and angiogenesis [35]. Within the SFKs, Src, Fyn, Yes and Lyn have all been shown to be involved in the GBM-related signaling [35]. Fyn and Src are described by Lu et al. as important players in the EGFR and EGFRvIII intracellular signaling [36]. By in vivo GBM knock-down experiments in mice, Lewis-Tuffin et al. demonstrated that Yes kinase affects tumor cell biology in a pro-tumorigenic manner, whereas Lyn acts in anti-tumorigenic way [35]. Moreover, Kleber et al. identified the involvement of Yes kinase in the induction of the invasion phenotype of GBM cells [37]. Indeed, upon the binding of CD95 Ligand to the CD95 receptor, Yes kinase is recruited to cellular membrane where it associates with the p85 subunit of PI3K (phosphatidylinositol 3-kinase), leading to the expression of matrix metalloproteinases (MMPs) and promoting tumor invasion [37].

Lck kinase, another member of SFKs, has been recently demonstrated to be involved in glioma progression at different levels by promoting the migration of GBM cells and tumor growth, and by regulating cancer cells stemness [38]. In addition, Lck is involved in the resistance of glioma stem cells to cisplatin and to fractionated radiations. The latter, indeed, has been demonstrated by Bommhardt et al. to increase the activity of Lck in glioma cells, but not of other SKFs, facilitating the expansion of the cancer stem cell population and enhancing GBM aggressiveness [39]. Interestingly, in

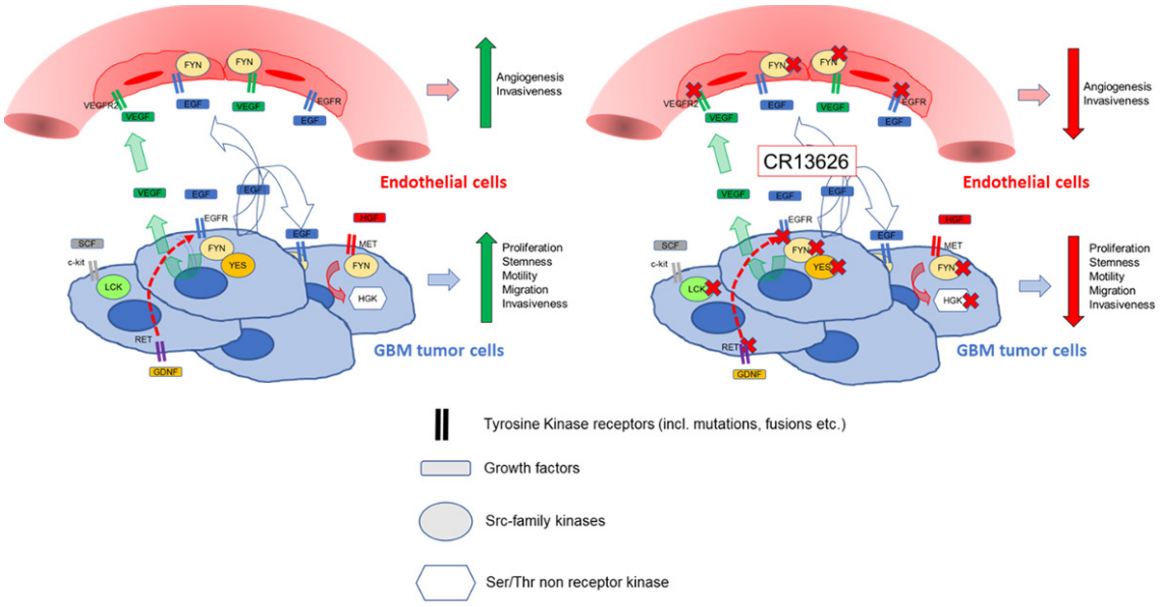

Figure 8. Proposed mechanisms by which CR13626 could act in GBM. The treatment with CR13626 could act both on endothelial and GBM tumor cells through the inhibition of VEGFR2 and EGFR and the downstream kinase Fyn, leading to a diminished tumor cells proliferation, migration, and counteracting the angiogenesis process. On GBM tumor cells, CR13626 can block the constitutively active form of EGFR receptor (EGFR vIII), which is the most frequent deletion occurring in GBM. Moreover, the inhibition of Yes kinase could contribute to a less invasion phenotype of GBM. By acting on the Lck kinase downstream the activated c-kit receptor, CR13626 could reduce cancer cells stemness and counteract the GBM resistance to TMZ. The inhibition of Fyn and HGK kinases could impair the c-MET receptor signaling pathway and decrease GBM migration and invasion. Finally, CR13626 could counteract one of the EGFR resistance mechanisms by blocking RET kinase.

small cell lung cancer Lck mediates the signal of c-kit receptor upon its activation by the stem cell factor (SCF) ligand [40], another system that seems to be involved in GBM resistance to TMZ [34].

Prolo et al. identified the HGK (aka MAP4K4) serine/threonine kinase as the strongest regulator of GBM invasion, whose expression is mostly upregulated by EGFRvIII compared to the wild-type EGFR [41]. The increased HGK activity in GBM cells may promote migration and invasion by reducing the expression of cell-cell adhesion molecule and directly activating proteins involved in cytoskeletal rearrangements [41]. Moreover, HGK activation downstream to the c-MET receptor is an emerging driving mechanism for medulloblastoma motility and invasiveness [42, 43].

CR13626 shows in vitro inhibitory activity against all the kinases above mentioned, allowing the compound to potentially act on several aspects of GBM tumor.

Moreover, CR13626 inhibits the RET receptor tyrosine kinase, which is overexpressed in several cancers, including glioma [44]. Most importantly, RET overexpression and fusions are acknowledged mechanisms related to EGFR resistance in many tumors, and are recently associated also with GBM [15, 45-48].

Thus, CR13626 could well represent the multi-kinase inhibitor acting on several targets at once described by Frantz [25]. The proposed mechanisms by which CR13626 could act in GBM is described in **Figure 8**.

CR13626 reduces the proliferation of different human GBM cell lines harboring some of the genetic alterations/mutations present in GBM tumor, including the temozolomide resistant cells (T98G), suggesting a potential broad activity of the compound and encouraging a further analysis in patient derived GBM primary cells. At the same time, CR13626 does not demonstrate toxicity in a non-tumoral cell line (HEK-293).

The presence of the blood brain barrier with efflux transporters, is one of the obstacles that must be overcome by a drug compound to achieve therapeutic concentrations. CR13626

is orally bioavailable (72%) and readily crosses the BBB in CD1 mice, without being a substrate of the multidrug efflux transporters. CR13626 demonstrates relevant brain penetration when dosed orally in mice, with a brain/plasma ratio of 1.4. The brain tropism and the exposure of animals to CR13626 are also confirmed in tumor bearing mice obtained by the injection of U87MG-Luc cells into the mouse brain. In the same orthotopic model of GBM, the oral treatment with CR13626 leads to a time-dependent reduction of tumor growth, which translates into a significant increase of the median survival time of the animals.

Taking together, such evidence warrants the further development of CR13626 as a potential new drug candidate in GBM.

Acknowledgements

This study was funded by Rottapharm Biotech. Rottapharm Biotech as a corporate entity had no role in the conduct of the study; in the collection, analysis, and interpretation of data; in the writing of the manuscript; or in the decision to submit the manuscript for publication.

Disclosure of conflict of interest

All the authors were employees of Rottapharm Biotech when the experiments had been performed.

Address correspondence to: Gianfranco Caselli, Rottapharm Biotech, Via Valosa di Sopra 9, Monza 20900, Italy. Tel: +39 039 9066059; Fax: +39 039-9066161; E-mail: gianfranco.caselli@rottapharmbiotech.com

References

[1] Oronsky B, Reid TR, Oronsky A, Sandhu N and Knox SJ. A review of newly diagnosed glioblastoma. Front Oncol 2021; 10: 1-10.

[2] Paolillo M, Boselli C and Schinelli S. Glioblastoma under siege: an overview of current therapeutic strategies. Brain Sci 2018; 8: 15.

[3] Stupp R, Mason WP, van den Bent MJ, Weller M, Fisher B, Taphoorn MJB, Belanger K, Brandes AA, Marosi C, Bogdahn U, Curschmann J, Janzer RC, Ludwin SK, Gorlia T, Allgeier A, Lacombe D, Cairncross JG, Eisenhauer E and Mirimanoff RO. European organisation for research and treatment of cancer brain tumor and radiotherapy groups, national cancer Institute of canada clinical trials group, radiotherapy plus concomitant and adjuvant temozolomide for glioblastoma. N Engl J Med 2005; 352: 987-96.

[4] Koshy M, Villano JL, Dolecek TA, Howard A, Mahmood U, Chmura SJ, Weichselbaum RR and McCarthy BJ. Improved survival time trends for glioblastoma using the SEER 17 population-based registries. J Neurooncol 2012; 107: 207-212.

[5] Thakkar JP, Dolecek TA, Horbinski C, Ostrom QT, Lightner DD, Barnholtz-Sloan JS and Villano JL. Epidemiologic and molecular prognostic review of glioblastoma. Cancer Epidemiol Biomarkers Prev 2014; 23: 1985-1996.

[6] Ostrom QT, Gittleman H, Truitt G, Boscia A, Kruchko C and Barnholtz-Sloan JS. CBTRUS statistical report: primary brain and other central nervous system tumors diagnosed in the United States in 2011-2015. Neuro Oncol 2018; 20: iv1-iv86.

[7] Burnet NG, Jefferies SJ, Benson RJ, Hunt DP and Treasure FP. Years of life lost (YLL) from cancer is an important measure of population burden-and should be considered when allocating research funds. Br J Cancer 2005; 92: 241-245.

[8] Patel AP, Tirosh I, Trombetta JJ, Shalek AK, Gillespie SM, Wakimoto H, Cahill DP, Nahed BV, Curry WT, Martuza RL, Louis DN, Rozenblatt-Rosen O, Suvà ML, Regev A and Bernstein BE. Single-cell RNA-seq highlights intratumoral heterogeneity in primary glioblastoma. Science 2014; 344: 1396-401.

[9] Pearson JRD and Regad T. Targeting cellular pathways in glioblastoma multiforme. Signal Transduct Target Ther 2017; 2: 1-11.

[10] Han X, Zhang W, Yang X, Wheeler CG, Langford CP, Wu L, Filippova N, Friedman GK, Ding Q, Fathallah-Shaykh HM, Gillespie GY and Nabors LB. The role of Src family kinases in growth and migration of glioma stem cells. Int J Oncol 2014; 45: 302-310.

[11] Alifieris C and Trafalis DT. Glioblastoma multiforme: pathogenesis and treatment. Pharmacol Ther 2015; 152: 63-82.

[12] Eskilsson E, Røsland GV, Solecki G, Wang Q, Harter PN, Graziani G, Verhaak RGW, Winkler F, Bjerkvig R and Miletic H. EGFR heterogeneity and implications for therapeutic intervention in glioblastoma. Neuro Oncol 2018; 20: 743-752.

[13] Gao Y, Vallentgoed WR and French PJ. Finding the right way to target EGFR in glioblastomas; lessons from lung adenocarcinomas. Cancers 2018; 10: 489.

[14] Warta R and Herold-Mende C. Helping EGFR inhibition to block cancer. Nat Neurosci 2017; 20: 1035-1037.

[15] Pan PC and Magge RS. Mechanisms of egfr resistance in glioblastoma. Int J Mol Sci 2020; 21: 1-21.

[16] Van Cruijsen H, Giaccone G and Hoekman K. Epidermal growth factor receptor and angiogenesis: opportunities for combined anticancer strategies. Int J Cancer 2005; 117: 883-888.
[17] Niclou SP. Revival of the VEGF ligand family? Neuro Oncol 2018; 20: 1421-1422.
[18] Lu-Emerson C, Duda DG, Emblem KE, Taylor JW, Gerstner ER, Loeffler JS, Batchelor TT and Jain RK. Lessons from anti-vascular endothelial growth factor and anti-vascular endothelial growth factor receptor trials in patients with glioblastoma. J Clin Oncol 2015; 33: 1197-1213.
[19] Gacche RN. Compensatory angiogenesis and tumor refractoriness. Oncogenesis 2015; 4: e153.
[20] Carmeliet P and Jain RK. Principles and mechanisms of vessel normalization for cancer and other angiogenic diseases. Nat Rev Drug Discov 2011; 10: 417-427.
[21] Tamura R, Tanaka T, Akasaki Y, Murayama Y, Yoshida K and Sasaki H. The role of vascular endothelial growth factor in the hypoxic and immunosuppressive tumor microenvironment: perspectives for therapeutic implications. Med Oncol 2020; 37: 2.
[22] Ganipineni LP, Danhier F and Préat V. Drug delivery challenges and future of chemotherapeutic nanomedicine for glioblastoma treatment. J Control Release 2018; 281: 42-57.
[23] Khaddour K, Johanns TM and Ansstas G. The landscape of novel therapeutics and challenges in glioblastoma multiforme: contemporary state and future directions. Pharmaceuticals 2020; 13: 1-26.
[24] Van Tellingen O, Yetkin-Arik B, De Gooijer MC, Wesseling P, Wurdinger T and De Vries HE. Overcoming the blood-brain tumor barrier for effective glioblastoma treatment. Drug Resist Updat 2015; 19: 1-12.
[25] Frantz S. Playing dirty. Nature 2005; 437: 942-943.
[26] Lee G, Thangavel R, Sharma VM, Litersky JM, Bhaskar K, Fang SM, Do LH, Andreadis A, Van Hoesen G and Ksiezak-Reding H. Phosphorylation of tau by fyn: implications for alzheimer's disease. J Neurosci 2004; 24: 2304-2312.
[27] Xu H, Czerwinski P, Hortmann M, Sohn HY, Förstermann U and Li H. Protein kinase C α promotes angiogenic activity of human endothelial cells via induction of vascular endothelial growth factor. Cardiovasc Res 2008; 78: 349-355.
[28] Bijman MN, van Nieuw Amerongen GP, Laurens N, van Hinsbergh VW and Boven E. Microtubule-targeting agents inhibit angiogenesis at subtoxic concentrations, a process associated with inhibition of Rac1 and Cdc42 activity and changes in the endothelial cytoskeleton. Mol Cancer Ther 2006; 5: 2348-2357.
[29] Rugo HS, Herbst RS, Liu G, Park JW, Kies MS, Steinfeldt HM, Pithavala YK, Reich SD, Freddo JL and Wilding G. Phase I trial of the oral antiangiogenesis agent AG-013736 in patients with advanced solid tumors: pharmacokinetic and clinical results. J Clin Oncol 2005; 23: 5474-5483.
[30] Moyer JD, Barbacci EG, Iwata KK, Arnold L, Boman B, Cunningham A, DiOrio C, Doty J, Morin MJ, Moyer MP, Neveu M, Pollack VA, Pustilnik LR, Reynolds MM, Sloan D, Theleman A and Miller P. Induction of apoptosis and cell cycle arrest by CP-358,774, an inhibitor of epidermal growth factor receptor tyrosine kinase. Cancer Res 1997; 57: 4838-4848.
[31] Hennequin LF, Allen J, Breed J, Curwen J, Fennell M, Green TP, Lambert-van der Brempt C, Morgentin R, Norman RA, Olivier A, Otterbein L, Plé PA, Warin N and Costello G. N-(5-chloro-1,3-benzodioxol-4-yl)-7-[2-(4-methylpiperazin-1-yl) ethoxy]-5-(tetrahydro-2H-pyran-4-yloxy)quinazolin-4-amine, a novel, highly selective, orally available, dual-specific c-Src/Abl kinase inhibitor. J Med Chem 2006; 49: 6465-88.
[32] Motaln H, Koren A, Gruden K, Ramšak Ž, Schichor C and Lah TT. Heterogeneous glioblastoma cell cross-talk promotes phenotype alterations and enhanced drug resistance. Oncotarget 2015; 6: 40998-41017.
[33] Lee SY. Temozolomide resistance in glioblastoma multiforme. Genes Dis 2016; 3: 198-210.
[34] Zaman N, Dass SS, Du Parcq P, MacMahon S, Gallagher L, Thompson L, Khorashad JS and Limbäack-Stanic C. The KDR (VEGFR-2) genetic polymorphism Q472H and c-KIT polymorphism M541L are associated with more aggressive behaviour in astrocytic gliomas. Cancer Genomics Proteomics 2020; 17: 715-727.
[35] Lewis-Tuffin LJ, Feathers R, Hari P, Durand N, Li Z, Rodriguez FJ, Bakken K, Carlson B, Schroeder M, Sarkaria JN and Anastasiadis PZ. Src family kinases differentially influence glioma growth and motility. Mol Oncol 2015; 9: 1783-1798.
[36] Lu KV, Zhu S, Cvrljevic A, Huang TT, Sarkaria S, Ahkavan D, Dang J, Dinca EB, Plaisier SB, Oderberg I, Lee Y, Chen Z, Caldwell JS, Xie Y, Loo JA, Seligson D, Chakravari A, Lee FY, Weinmann R, Cloughesy TF, Nelson SF, Bergers G, Graeber T, Furnari FB, David James C, Cavenee WK, Johns TG and Mischel PS. Fyn and Src are effectors of oncogenic epidermal growth factor receptor signaling in glioblastoma patients. Cancer Res 2009; 69: 6889-6898.
[37] Kleber S, Sancho-Martinez I, Wiestler B, Beisel A, Gieffers C, Hill O, Thiemann M, Mueller W,

Sykora J, Kuhn A, Schreglmann N, Letellier E, Zuliani C, Klussmann S, Teodorczyk M, Gröne HJ, Ganten TM, Sültmann H, Tüttenberg J, von Deimling A, Regnier-Vigouroux A, Herold-Mende C and Martin-Villalba A. Yes and PI3K bind CD95 to signal invasion of glioblastoma. Cancer Cell 2008; 13: 235-248.

[38] Zepecki JP, Snyder KM, Moreno MM, Fajardo E, Fiser A, Ness J, Sarkar A, Toms SA and Tapinos N. Regulation of human glioma cell migration, tumor growth, and stemness gene expression using a Lck targeted inhibitor. Oncogene 2019; 38: 1734-1750.

[39] Bommhardt U, Schraven B and Simeoni L. Beyond TCR signaling: emerging functions of Lck in cancer and immunotherapy. Int J Mol Sci 2019; 20: 1-18.

[40] Krystal GW, DeBerry CS, Linnekin D and Litz J. Lck associates with and is activated by kit in a small cell lung cancer cell line: Inhibition of SCF-mediated growth by the Src family kinase inhibitor PP1. Cancer Res 1998; 58: 4660-4666.

[41] Prolo LM, Li A, Owen SF, Parker JJ, Foshay K, Nitta RT, Morgens DW, Bolin S, Wilson CM, Vega L JCM, Luo EJ, Nwagbo G, Waziri A, Li G, Reimer RJ, Bassik MC and Grant GA. Targeted genomic CRISPR-Cas9 screen identifies MAP4K4 as essential for glioblastoma invasion. Sci Rep 2019; 9: 14020.

[42] Santhana Kumar K, Tripolitsioti D, Ma M, Grählert J, Egli KB, Fiaschetti G, Shalaby T, Grotzer MA and Baumgartner M. The Ser/Thr kinase MAP4K4 drives c-Met-induced motility and invasiveness in a cell-based model of SHH medulloblastoma. Springerplus 2015; 4: 19.

[43] Tripolitsioti D, Kumar KS, Neve A, Migliavacca J, Capdeville C, Rushing EJ, Ma M, Kijima N, Sharma A, Pruschy M, McComb S, Taylor MD, Grotzer MA and Baumgartner M. MAP4K4 controlled integrin β1 activation and c-Met endocytosis are associated with invasive behavior of medulloblastoma cells. Oncotarget 2018; 9: 23220-23236.

[44] Mulligan LM. GDNF and the RET receptor in cancer: new insights and therapeutic potential. Front Physiol 2019; 10: 1-13.

[45] Lin C, Lu W, Ren Z, Tang Y, Zhang C, Yang R, Chen Y, Cao W, Wang L, Wang X and Ji T. Elevated RET expression enhances EGFR activation and mediates EGFR inhibitor resistance in head and neck squamous cell carcinoma. Cancer Lett 2016; 377: 1-10.

[46] Leonetti A, Sharma S, Minari R, Perego P, Giovannetti E and Tiseo M. Resistance mechanisms to osimertinib in EGFR-mutated non-small cell lung cancer. Br J Cancer 2019; 121: 725-737.

[47] Zhu VW, Klempner SJ and Ou SI. Receptor tyrosine kinase fusions as an actionable resistance mechanism to EGFR TKIs in EGFR-mutant non-small-cell lung cancer. Trends Cancer 2019; 5: 677-692.

[48] Woo HY, Na K, Yoo J, Chang JH, Park YN, Shim HS and Kim SH. Glioblastomas harboring gene fusions detected by next-generation sequencing. Brain Tumor Pathol 2020; 37: 136-144.

Table S1. Percent inhibition by CR13626 at 1 μM on 173 kinases (in = less than 50% inhibition)

Tyr kinases		*CR13626*
		% inhib @1 μM
RTK	Axl kinase	in
	c-kit kinase	in
	c-Met kinase	in
	DDR2 kinase	78.0%
	EphA1 kinase	in
	EphA2 kinase	in
	EphA3 kinase	in
	EphA4 kinase	in
	EphA5 kinase	in
	EphA7 kinase	in
	EphB1 kinase	50.6%
	EphB2 kinase	in
	EphB4 kinase	70.1%
	EGFR kinase	96.1%
	HER2/ErbB2 kinase	in
	FGFR1 kinase	80.5%
	FGFR3 kinase	85.7%
	FGFR2 kinase	75.8%
	FGFR4 kinase	in
	FLT-1 kinase (VEGFR1)	74.6%
	KDR kinase (VEGFR2)	101.0%
	FLT-3 kinase	80.2%
	FLT-4 kinase (VEGFR3)	96.4%
	PDGFRalpha kinase	72.9%
	PDGFRbeta kinase	59.6%
	IGF1R kinase	in
	IRK (InsR)	in
	Fms/CSFR kinase	70.3%
	IRR kinase	55.2%
	LTK	56.6%
	MusK	53.3%
	Ret kinase	95.6%
	Ron kinase	in
	TRKA	65.5%
	TRKB	in
	TRKC	66.4%
	Tyro3/Sky kinase	in
CTK	Abl kinase	84.1%
	Ack	92.6%
	Arg kinase	84.3%
	Brk	in
	FAK	in
	Fer kinase	in
	Fes kinase	in
	Fgr kinase	99.0%

	FRK	57.8%
	Fyn kinase	98.9%
	ITK	57.3%
	JAK1	in
	JAK2	in
	JAK3	in
	Lck kinase	89.8%
	Lyn A kinase	99.0%
	Lyn B kinase	in
	PYK2	in
	Src kinase	90.6%
	Syk	in
	Tnk1	in
	TXK	76.1%
	Tyk2 (JTK1)	in
	Yes kinase	99.0%
	ZAP70 kinase	94.5%

Table S2. Percent inhibition by CR13626 at 1 μM on 173 kinases (cont.)

Ser/Thr kinases		*CR13626*
		% inhib @1 μM
CMGC	CDC2/CDK1 (cycB)	in
	CDK2 (cycA)	in
	CDK3 (cycE1)	in
	CK2 (casein kinase 2)	in
	CDK4 (cycD1)	60.8%
	CDK6 (cycD3)	74.1%
	CDK7/MAT1 (cycH)	in
	CDK8 (cycC)	in
	CDK9 (cycT1)	in
	CLK1	in
	DYRK1a	in
	DYRK2	in
	ERK1	in
	ERK2 (P42mapk)	in
	GSK3alpha	in
	GSK3beta	in
	HIPK2	in
	JNK1	in
	JNK3	in
	p38alpha kinase	82.7%
	p38delta kinase	in
CaMK	AMPKalpha	74.2%
	BRSK1	in
	CaMK1delta	63.4%
	CaMK2alpha	in
	CaMK4	in

	CHK1	in
	CHK2	in
	DAPK2	in
	DCAMKL1	in
	DCAMKL2	in
	DRAK1	in
	MAPKAPK2	in
	MAPKAPK5 (PRAK)	in
	MARK1	in
	MARK3	in
	MNK1	in
	MNK2	in
	NIM1 kinase (MGC42105)	in
	NuaK1 (ARK5)	in
	PhKgamma 1	in
	PhKgamma2	in
	Pim1 kinase	in
	Pim2 kinase	in
	SIK	in
	STK33	in
	TSSK1	in
AGC	Akt1/PKBalpha	in
	Akt2/PKBbeta	in
	Akt3/PKBgamma	in
	CRIK	in
	GRK2 (ADRBK1)	in
	GRK3/BARK2 (ADRBK2)	in
	MSK2	in
	NDR1 kinase	in
	p70S6K	in
	p70S6Kbeta	in
	PDK1	in
	PKA	in
	PKCalpha	in
	PKCbeta 2	in
	PKN1	in
	PRKX	in
	ROCK1	in
	ROCK2	in
	RSK1	in
	RSK2	in
	RSK3	in
	SGK1	in
	SGK3	in
STE	COT kinase (MAP3K8)	in
	GCK (MAP4K2)	67.9%
	HGK (MAP4K4)	99.3%
	MEK5 (MAP2K5)	in

	MEKK3 (MAP3K3)	68.3%
	MEKK4 (MAP3K4)	53.5%
	MST1 kinase (STK4)	in
	MST3 kinase	in
	NIK	in
	PAK2	in
	PAK4	in
	TAOK2 (TAO1)	in
TKL	ALK4 (ACVR1B)	72.2%
	BMPR1A (ALK3)	63.2%
	B-Raf kinase	in
	DLK1 (MAP3K12)	in
	IRAK1	in
	IRAK4	in
	LIMK1	in
	MLK1	in
	MLK2 (MAP3K10)	in
	RAF-1 kinase	in
	RIPK2	62.1%
	TAK1-TAB1 (MAP3K7)	in

Table S3. Percent inhibition by CR13626 at 1 μM on 173 kinases (cont.)

Other kinases		*CR13626*
		% inhib @1 μM
	AurA/Aur2 kin	in
	IKKalpha	in
	IKKbeta	in
	IKKepsilon (IKBKE)	in
	NEK2	in
	NEK4	in
	NEK6	in
	PEK (EIF2AK3)	in
	PLK1	in
	PLK2	in
	TBK1	in
	TTK	in
	ULK1	in
	Wee1 kinase	61.8%
	WNK2	77.4%
	WNK3	75.0%
	WNK4	in

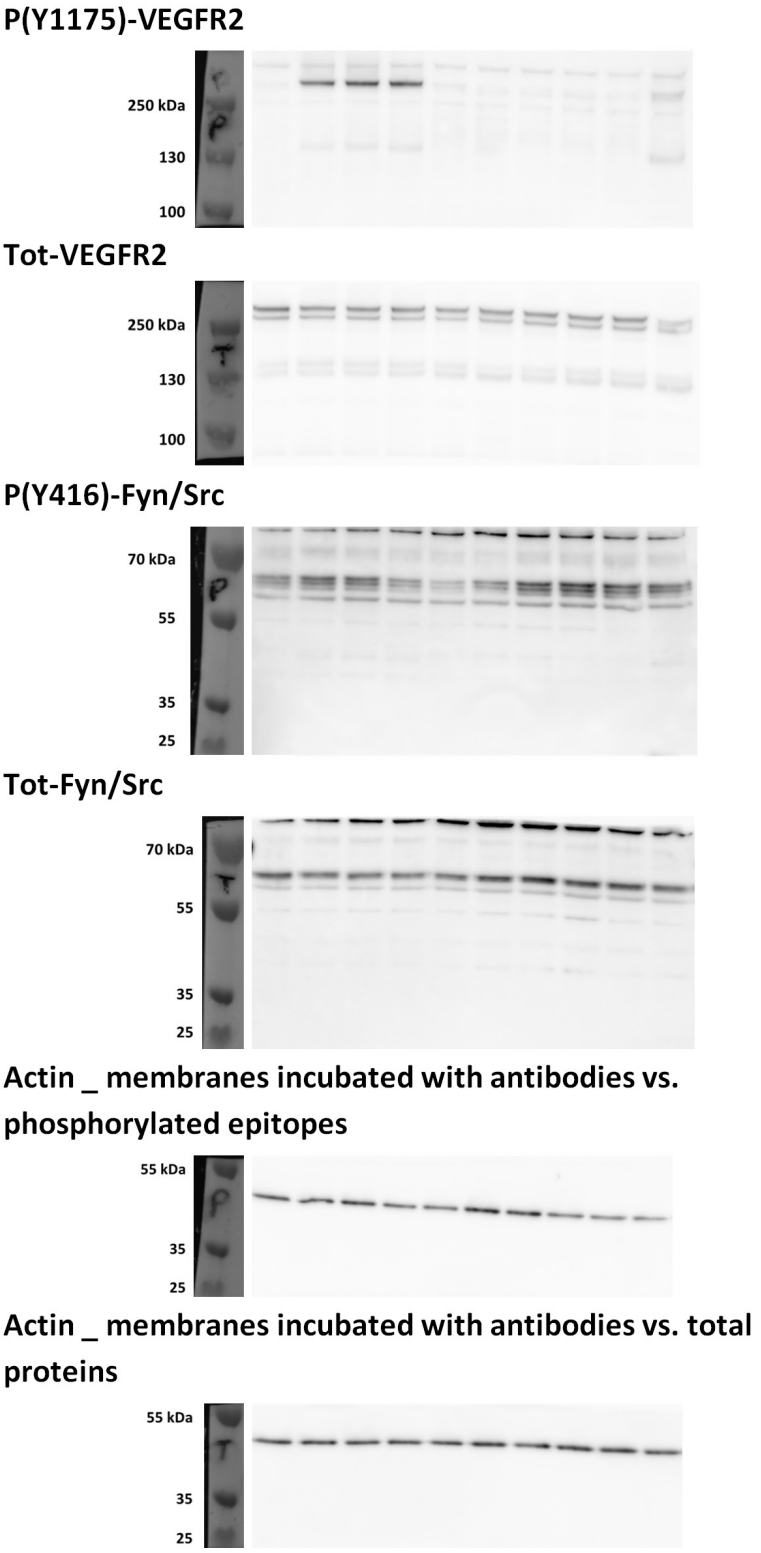

Figure S1. Immunoblot analysis of VEGFR2 phosphorylation on tyrosine residue 1175 (P(Y1175)), total VEGFR2 (Tot-VEGFR2), Fyn/Src phosphorylation on tyrosine residue 416 (P(Y416)), total Fyn (Tot-Fyn) and Actin (loading control) in human HUVEC-C cell lysates.

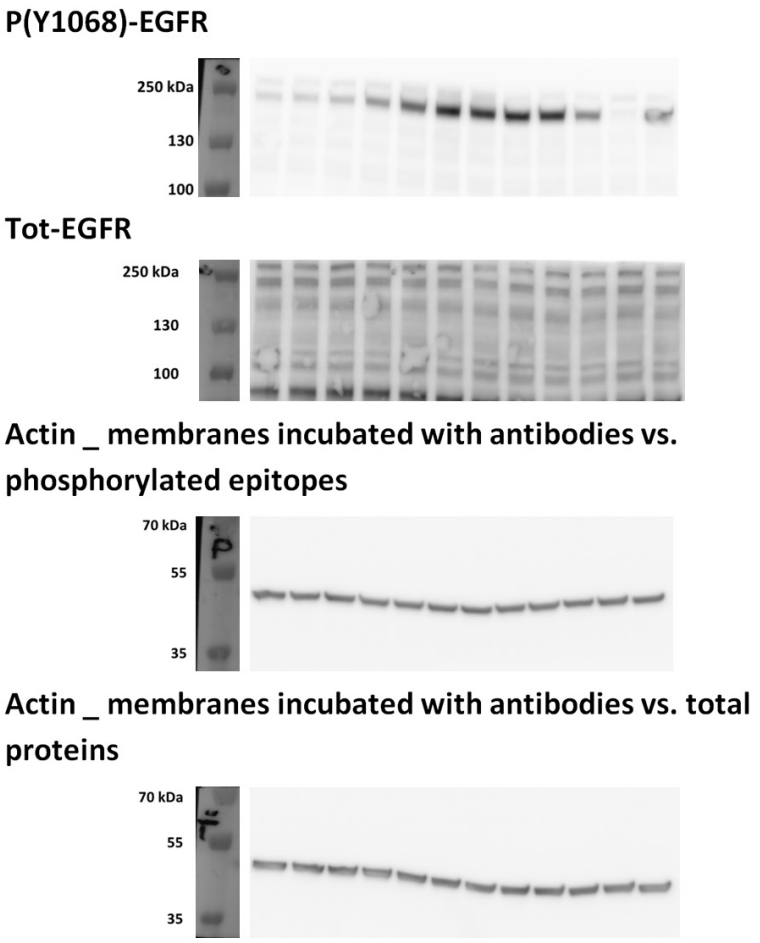

Figure S2. Immunoblot analysis of EGFR phosphorylation on tyrosine residue 1068 (P(Y1068)), total EGFR (TOT-EGFR), and Actin (loading control) in human GBM U87MG cell lysates.